Diamond & Related Materials 98 (2019) 107520

Contents lists available at ScienceDirect

Diamond & Related Materials

journal homepage: www.elsevier.com/locate/diamond

Co-deposition of diamond and β-SiC by microwave plasma CVD in H_2-CH_4-SiH_4 gas mixtures

V.S. Sedov[a,*], A.K. Martyanov[a], A.A. Khomich[a,b], S.S. Savin[c], V.V. Voronov[a], R.A. Khmelnitskiy[d], A.P. Bolshakov[a,e], V.G. Ralchenko[a,e,f]

[a] Prokhorov General Physics Institute, Russian Academy of Sciences, Moscow 119991, Russia
[b] Institute of Radio Engineering and Electronics, Russian Academy of Sciences, Fryazino 141190, Russia
[c] Moscow Technological University, Moscow 119454, Russia
[d] Lebedev Physical Institute, Russian Academy of Sciences, Moscow 119991, Russia
[e] National Research Nuclear University MEPhI, Moscow 115409, Russia
[f] Harbin Institute of Technology, Harbin 150001, PR China

ARTICLE INFO

Keywords:
CVD diamond
Silicon carbide
Composite
Microwave plasma
Silane

ABSTRACT

The co-deposition of diamond and silicon carbide (SiC) was realized in a microwave plasma using H_2-CH_4-SiH_4 mixtures at enhanced microwave power density of up to 150 W/cm^3, and SiC/diamond composite films on (100) Si substrates were produced. The growth parameters were selected to ensure almost equal deposition rates of ~0.3 μm/h for both phases. Composite films were formed either directly on Si surface, or on a buffer (nucleation) layer of SiC or diamond, preliminary deposited on the Si substrate. The film structure has been characterized by SEM, XRD, Raman and PL spectroscopy. It was confirmed that the silicon carbide phase in the composite is the cubic polytype β-SiC (3C-SiC) with the presence of only a small fraction of the hexagonal polytype, while the diamond is in well-faceted microcrystalline form. Diamond grains are Si-doped as was evidenced by the strong photoluminescence of silicon-vacancy color centers. Also, minor inclusions of amorphous sp2 carbon and of *trans*-polyacetylene (t-PA) were detected in the β-SiC phase. The overall crystalline quality of the composite is high, as evidenced by narrow Raman peaks both for diamond and β-SiC. Our results show, that with an appropriate choice of growth parameters, particularly SiH_4/CH_4 ratio, high-quality films of Si-doped diamond, silicon carbide, SiC-diamond composite, and combinations of these structures can be synthesized in a single process.

Prime novelty statement: The co-deposition of diamond and SiC was realized by microwave plasma CVD using H_2-CH_4-SiH_4 mixtures at enhanced microwave power density; β-SiC/diamond composite films were produced with high crystalline quality on (100) Si substrates.

1. Introduction

Diamond/silicon carbide composites, consisting of the two wide-bandgap materials, each with excellent thermal, electronic, optical, and mechanical properties, are of high interest to a number of important applications, such a superhard cutting tools and protective layers [1–4], heat spreaders (with tuned thermal expansion coefficient) for high power electronic devices [5,6], field electron emitters [7], selective protein absorbent in medical applications [8]. The availability of bright color centers both in diamond [9] and SiC [10] as single-photon emitters makes such composites interesting also for quantum information technologies.

Different methods to produce diamond/SiC composites are reported in literature. First, the bulk composites were sintered at high pressures (2–8 GPa) and high temperatures by a molten Si infiltration into a diamond powder compact, with the Si-diamond reaction to form SiC in voids between diamond grains [2,11,12]. A limited size of the produced composites and an incomplete conversion of Si to SiC are disadvantages of the technique. Another approach relies on the liquid Si infiltration at low pressures into pores of a diamond compact (green body) to form SiC via the Si−C reaction, achieving the diamond fraction as high as 50–70% in the produced diamond/SiC composite [5,13]. However, the stress and the formation of turbostratic carbon on SiC–diamond interfaces, which may reduce the thermal conductivity of the material, have been revealed in this type of the composite [13]. Moreover, the Si infiltration was possible only for large enough diamond grain size

* Corresponding author.
E-mail address: sedovvadim@yandex.ru (V.S. Sedov).

https://doi.org/10.1016/j.diamond.2019.107520
Received 19 July 2019; Received in revised form 15 August 2019; Accepted 20 August 2019
Available online 22 August 2019

(typically > 10–20 μm), preventing the formation of highly uniform finely dispersed composites. Pores in diamond compacts can be filled in a vacuum with Si vapors at 1600 °C, resulting in the reactive formation of SiC binder, however, with the incomplete Si to SiC transformation [14]. In addition, the fabrication of composites Si/SiC-diamond by the electrospark assisted reactive sintering was reported [15].

In order to overcome problems with the residual porosity and the presence of carbon and/or Si inclusions on interfaces, the promising alternative approach to fabricate SiC/diamond composites by a chemical vapor deposition (CVD) process was developed by Jiang's group [16–20]. The composite was produced by a microwave plasma CVD (MPCVD) in H_2-CH_4-tetramethylsilane ($Si(CH_3)_4$, TMS) mixtures via co-deposition of diamond and cubic polytype β-SiC (3C-SiC). The composite structure can be (a) nanocrystalline, when the film is grown at low absorbed microwave power density (MWPD), and (b) microcrystalline, with a better quality of both phases, at high MWPD (of the order of 30 W/cm^3) [18]. The possibility to fabricate large area diamond-SiC composite films on both planar- and complex-shaped substrates makes such CVD technique advantageous for a wide range of applications. The main challenge is to find the deposition parameters, when both diamond and β-SiC components growth with the same rate, otherwise one of them will eventually dominate. While few percent of methane in H_2 is typical for diamond deposition process, the addition of rather low TMS concentrations of about 0.01 at.% to CH_4-H_2 gas mixtures can be enough to make β-SiC formation competitive and to obtain mixed diamond/β-SiC films [17]. Using TMS as the Si (and also C) precursor with low TMS concentration (1–3% TMS vs CH_4 and ~1% CH_4 vs H_2), the growth rates of the order of 100 nm/h for the diamond-SiC composite films were reported [18,19].

Another suitable silicon-containing gas precursor for obtaining SiC films by MPCVD is silane SiH_4, added to H_2-CH_4 mixtures, also in a small quantity (< 1%) [21]. Earlier, we demonstrated the efficient in situ doping of both polycrystalline [22] and single-crystal diamond [23] with Si at very low percentage of silane in CH_4-H_2 process gas (SiH_4/CH_4 < 1%, SiH_4/H_2 < 0.06%) in the course of the diamond films deposition in a MPCVD reactor. Using TMS as the precursor limits the SiC deposition process by the Si/C ratio of 0.25 in the gas (in TMS-CH_4-H_2 mixtures) at most because the Si and C sources are combined in one molecule. In contrast, using CH_4 and SiH_4 as two separate precursors allows much broader choice for Si/C ratio, from zero to infinity, which promises a potential advantage of silane for the growth of SiC, Si-doped diamond and pure Si films, as well as SiC-diamond composites, multilayered and gradient structures. However, the appropriate deposition regimes to obtain SiC-diamond composites in silane-containing gases are not established so far.

In the present work, being inspired by potential applications of such composite films as adhesive interlayers for tool coatings, thermal management in electronic devices, and photoluminescence sources, we explored simultaneous growth of diamond and SiC phases by MPCVD with H_2-CH_4-SiH_4 mixtures at high silane contents and enhanced microwave power density. We produced diamond-SiC composite films with two different buffer layers (single-phase diamond or single-phase SiC) on Si substrates in one process, and characterized their structure.

2. Experimental

The diamond and SiC co-deposition was performed in the MPCVD system ARDIS-100 (2.45 GHz) [22,24] in CH_4-H_2-SiH_4 gas mixtures as shown schematically in Fig. 1. Single-crystalline (100)-oriented polished silicon wafers 10 × 10 × 0.5 mm^3 in size were used as the substrates for growth of the diamond/SiC films. Prior to the deposition, the substrates were seeded with nanodiamond (ND) particles using ultrasonic treatment for 10 min in an isopropanol suspension of the ND powder with the average size of 50 or 200 nm (Tomei Diamond) to provide diamond nucleation centers. The ND concentration in the suspension could be varied to tune the nucleation areal density.

The substrate was then transferred to the CVD reactor, being placed in a central zone of a Mo substrate holder of 57 mm in diameter. The deposition process was carried out at pressures of 60–80 Torr, microwave power of 2.8–4.5 kW, total gas flow rate of 500 sccm and the substrate temperature of 750–875 °C as measured with a two-color pyrometer (Willamson 81-35-C) through the top quartz window of the CVD reactor. The concentrations of gaseous precursors were selected in the range of SiH_4/CH_4 = 10–20% and CH_4/H_2 = 4%, while the deposition time varied from 5 to 100 h. In addition to the simple scheme shown in Fig. 1 two other versions of the growth process of the composite films were studied aimed to facilitate the nucleation either for SiC or diamond on the substrate. The process modification included a preliminary deposition of appropriate buffer layer directly on the Si substrate. The first type of the interlayer was a thin β-SiC film produced in H_2-CH_4-SiH_4 mixture. At the next step, the β-SiC interlayer was densely seeded with ND particles, and the SiC-diamond co-deposition proceeded in H_2-CH_4-SiH_4 mixture. The second type of interlayer was a diamond film grown in H_2-CH_4 mixture on densely seeded Si substrate. Then, the SiC-diamond composite was deposited in the H_2-CH_4-SiH_4 gas mixture: the diamond grains continued to grow epitaxially on the diamond interlayer in-between spontaneously nucleated particles of SiC.

The microwave power density P/V, defined as an absorbed power P divided by a plasma ball volume V, was evaluated by profiling the atomic hydrogen H_α line intensity on photographs captured with the digital mirror camera Canon EOS 650D equipped with the monochromatic optical filter with λ~656 nm, that allows only the Hα-emission from plasma to be registered (see more details on the used technique in [25]). Spatial intensity $I_{H\alpha}$ profiles were fit with Gaussian profiles, and the volume was calculated assuming the plasma to have an ellipsoid shape. The MWPD as high as 150 W/cm^3 was determined for the typical growth regimes with P = 4.0 kW, several times higher compared to MWPD values used in experiments by Jiang et al. [18,19].

The thickness and the growth rate of diamond and SiC films obtained at different process parameters were measured in-situ with a laser interferometry technique [26]. The laser beam ($\lambda = 650\,nm$) was directed almost perpendicularly to the growing surface through the top quartz window of the CVD reactor. The reflected beam was collected and directed to the optical spectrometer Ocean Optics 4000 through the same window. The thickness of the film increases by $\Delta h = \lambda/2n$ for one period of the reflected beam intensity oscillations, where n is refraction index of the material (the increment Δh is 134.5 nm for diamond and 127.5 nm for SiC). In view of the proximity of the refraction index for diamond and SiC ($n \approx 2.4$), the error in evaluation of the composite film thickness could be about 5% or even less, if the average Δh_{av} = 131 nm is adopted.

The phase composition of the obtained diamond-SiC films was analyzed at room temperature with micro-Raman spectroscopy using LABRAM HR-800 spectrometer equipped with a diode-pumped solid-state laser (λ = 473 nm). The spectrometer operated in a confocal mode, while laser beam was focused in a spot of ≈1 μm in diameter of the sample surface, was also used for measurement of photoluminescence (PL) spectra for the samples. X-ray diffraction (XRD) measurements were performed with the Bruker D8 Discover A25 DaVinsi Design instrument (CuKα radiation at 40 kV voltage, focus spot size of 0.4 × 12 mm^2) in two modes: (a) in Bragg–Brentano geometry in the 2θ range of 20–140° with a step size of 0.02° and the exposition time of 1 s for a single step, and (b) at grazing incidence diffraction. XRD spectra were processed with the EVA 1.0 software and analyzed using the PDF-2 database. The film surface morphology and the grain size were examined with scanning electron microscopy (SEM) using instruments JEOL JSM7001F and Tescan MIRA3 (with Energy-dispersive X-ray spectroscopy module, EDX).

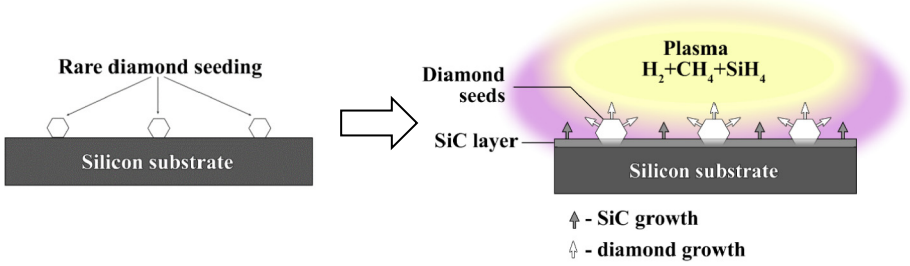

Fig. 1. Schematics for the Si substrate seeding with ND particles and the growth of the SiC-diamond composite: (a) rare diamond seeding on a silicon substrate and (b) simultaneous deposition of diamond and SiC phases.

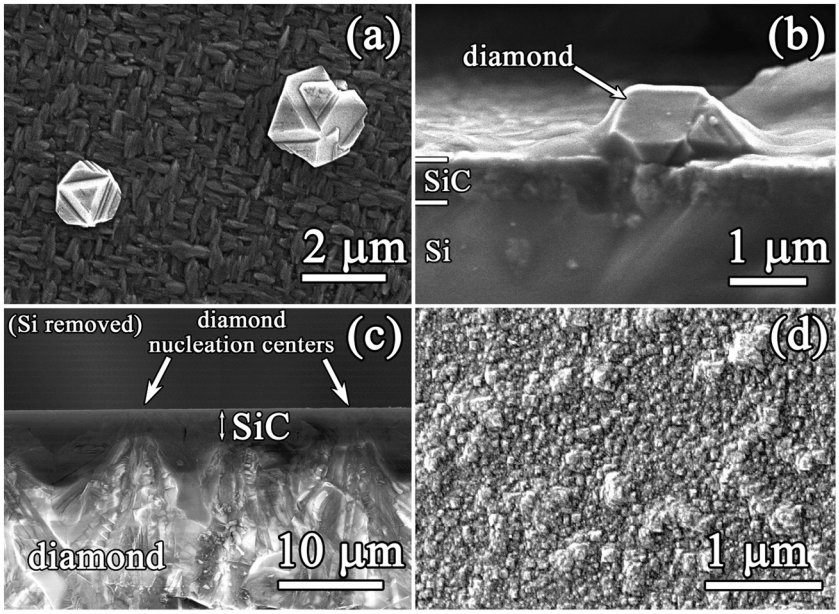

Fig. 2. SEM images of the textured SiC/diamond film deposited on the Si substrate in the H_2-CH_4-SiH_4 mixture in a regime with the higher growth rate for the diamond component than that for the SiC one: pressure of 70 Torr, microwave power of 2.8 kW, substrate temperature of 800 °C, SiH_4/CH_4 = 10%, CH_4/H_2 = 4%. (a) plan-view and (b) cross-section of 550 nm thick SiC/diamond film deposited for 5 h on the Si substrate with low nucleation density. The textured film is β-SiC, the faceted crystals are diamond. (c) Cross-section of the SiC/diamond film grown for 100 h at the same process parameters. The Si substrate was chemically removed; the nucleation side is shown on top of the image. The primarily dominating SiC layer is completely buried in the overgrown diamond film. (d) Nucleation side of the free-standing composite film (plan view).

3. Results and discussion

3.1. Si/SiC-diamond composite

The plan-view SEM image of the film produced on intentionally poorly seeded Si substrate (200 nm ND with concentration of 1 mg/l in suspension) for 5 h growth time (MW power 2.8 kW, pressure 70 Torr, 4% CH_4, 10% Si/C, substrate temperature 800 °C) is shown in Fig. 2a. The main part of the continuous film displays a "fabric-like" highly textured structure that is characteristic for heteroepitaxial growth of β-SiC on Si [21,27]. Also, some well-faceted twinned diamond crystals grown to sizes of up to ~2 μm, and protruding from SiC film (Fig. 2a). The cross-section of the sample reveals the SiC film with a thickness of ~550 nm (Fig. 2b), thus corresponding to the deposition rate of 110 nm/h. The presence of an isolated diamond crystal with the height of about 1.5 μm allows an assessment of the diamond growth rate of 260 nm/h (the seed size of 200 nm was taken into account in this estimate), a doubled rate compared to that for SiC phase.

Due to the significant difference in the growth rates for the two components, after a longer process time, the SiC film turned out to be buried in the diamond film as a result of lateral spread of the latter. Eventually, a continuous diamond film is formed on the top of Si/SiC/diamond structure. The SEM image of the cross-section of such thick film (29 μm) produced in the course of the 100 h deposition run under the process parameters identical (keeping nucleation density low) to those for the thin film, is shown in Fig. 2c. The Si substrate was etched in HNO_3 + HF acid solution to allow inspection of the nucleation side of the composite film, which is shown here on the top of the image. The cross-section reveals a nonuniform, gradient structure of the composite material, with diamond grains fan out from nucleation rear centers due to 3D growth. The expected positions of diamond nucleation centers are apexes of the conically expanded diamond grains, as pointed out with arrows. While the typical distance between nucleation centers is large enough (5–10 μm), the higher deposition rate of the diamond phase eventually led to the complete overgrowth of diamond grains over the SiC layer, so only the PCD layer was observed on the growth surface after the first 5–10 μm thick composite layer is formed. The SiC nucleation layer on the substrate side (Fig. 2d) exhibits fine surface features with typical dimensions of 50 nm or less. The diamond nucleation centers are relatively rare, and hardly can be recognized among the dominating SiC grains on the small scale image in Fig. 2d. The nucleation surface is rather smooth with roughness R_{rms} = 6 nm as measured with Zygo NewView 5000 optical profilometer on the arbitrary selected area of 263 × 197 μm^2.

The Raman spectrum for the SiC film (Fig. 2a), taken in the area far from isolated diamond grains, is displayed in Fig. 3a. The strong sharp peak at 796 cm^{-1} belongs to the TO-phonon mode of the cubic polytype of silicon carbide – β-SiC (3C-SiC), while the shoulder on its lower wavenumbers slope is caused by the presence of a weak peak at 766 cm^{-1} of the TO-phonon mode of hexagonal polytype 6H-SiC [28]. In addition, a weak band assigned to LO-phonon mode for β-SiC appears at 820–970 cm^{-1}. We conclude that the SiC film grown on Si (100) has β-SiC structure with the presence of a small fraction of the hexagonal polytype.

Other intensive features in the Raman spectrum are strong wide bands at 1350 cm^{-1} and 1590 cm^{-1} (D-peak and G-peak of amorphous

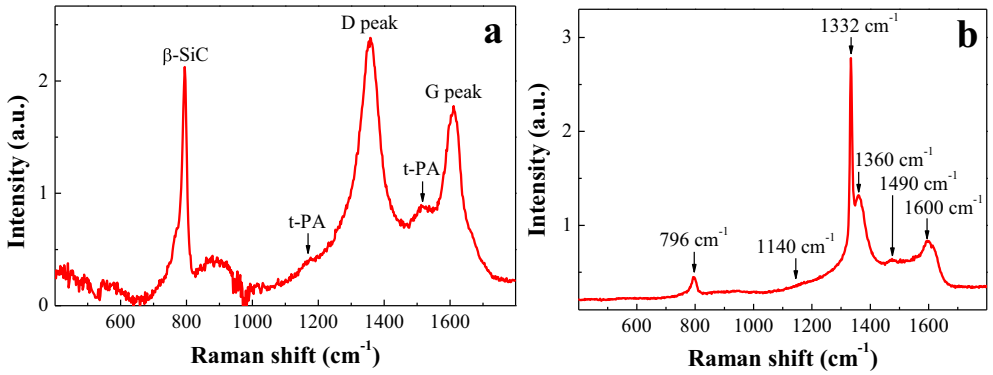

Fig. 3. Raman spectra for the SiC/diamond film with low nucleation density of diamond (see Fig. 2) for: (a) the SiC film in a zone far from diamond grains; (b) a single diamond grain. The Raman peak for Si at 520 cm^{-1} is subtracted from the measured spectra.

sp2 carbon) and two weak bands of *trans*-polyacetylene (t-PA) at 1140 cm^{-1} and 1480 cm^{-1}. We note that Zhuang et al. [27] reported the formation of amorphous sp2 carbon upon β-SiC deposition using H_2-TMS gas mixtures at elevated substrate temperatures (> 900 °C) or low microwave power densities. The formation of amorphous carbon inclusions and t-PA is typical for nanocrystalline diamond (NCD) films [29], and may indicate the localization of those inclusions on grain boundaries of oriented SiC crystallites similarly to the case of NCD. The sharp 1st order diamond Raman peak at 1333 cm^{-1} with the full width at half maximum (FWHM) of 7.6 cm^{-1}, observed for dispersed faceted crystals (see Fig. 2a), verifies them as diamond grains (Fig. 3b). We note that the Raman spectrum (not shown here) taken on nucleation side of the thick free-standing film (Fig. 2d) revealed the SiC peak and other features quite similar to those given for 5 h-grown thin film in Fig. 3.

3.2. Si/diamond/SiC-diamond composite

At the next step, the process parameters were tuned to equalize growth rates of diamond and SiC phases to allow the synthesis of thick composite films. With this aim, a three-layer composite sample was prepared. First, the Si substrate was densely seeded with ND particles (50 nm) by ultrasonic treatment, and then a pure polycrystalline diamond (PCD) film of ~7 μm thickness was deposited for 2 h at the microwave power of 4.5 kW, pressure of 80 Torr, substrate temperature 850 ± 25 °C, CH_4/H_2 = 4%. The growth rate for the diamond buffer layer was 3.5 μm/h, an order of magnitude higher compared to that for the SiC/diamond composite. Then, SiH_4 was added in the reactor, and the set of growth parameters was changed to: microwave power of 4.0 kW, pressure of 72 Torr, substrate temperature 775 ± 25 °C, $[CH_4]/[H_2]$ = 4%, and $[SiH_4]/[CH_4]$ = 20%, to continue the deposition process for next 20 h. This resulted in the formation of the 5.6 μm thick composite film with the growth rate of 280 nm/h. The SiC spontaneous nucleation took place directly on diamond surface, while diamond continued to grow epitaxially on the buffer PCD layer. The composite growth rate decrease is believed to be caused by a combined effect of lower substrate temperature, lower pressure, and influence of SiH_x radicals on the plasma and surface chemistry [19].

SEM images of the cross-section and plan view of the produced Si/diamond/SiC-diamond structure with the total thickness of 12.6 μm are displayed in Fig. 4a–e. The images are obtained in different modes: (i) secondary electrons (SE) mode, (ii) backscattered electrons (BSE) mode to enhance the contrast of different phases due to the high *Z*-contrast between carbon and silicon, and (iii) energy-dispersive X-ray spectroscopy (EDX) mapping mode for elemental analysis. The presence of SiC particles coexisting with diamond can be observed in the cross-section in the top half of the film (Fig. 4b, c). The plan view (Fig. 4d, e) demonstrates, that the SiC component is located mainly on grain boundaries of the diamond film, in valleys between the diamond crystallites. This observation indicates that (a) diamond grain boundaries with an enhanced abundance of defects and/or (b) facets with specific orientations, such as {111} surfaces [17], may be the preferential area for SiC nucleation. In contrast to diamond, the SiC domains look as aggregates of small, submicron SiC particles, as clearly seen in Fig. 4d.

Raman spectra for a diamond grain and a SiC inclusion are shown in Fig. 4f. The spectrum for the region with SiC particles displays the strong peak at 795.6 cm^{-1} with FWHM of 9.1 cm^{-1} assigned to TO-phonon mode of β-SiC cubic polytype [28,30]. Other features are similar to those observed in the spectrum for the highly-textured SiC film (Fig. 3a), and include D-peak (1350 cm^{-1}) and G-peak (1590 cm^{-1}) of amorphous graphitic carbon, diamond peak at 1332 cm^{-1} from the surrounding diamond matrix, and the t-PA band at 1140 cm^{-1}. Also, the weak 1st order Raman peak of Si (substrate) can be observed at 520 cm^{-1} due to partial optical transparency of the composite film. The Raman spectrum of a diamond grain is shown in the inset in Fig. 4f. It displays only the strong narrow (8.3 cm^{-1}) 1st order peak at 1332.2 cm^{-1}. No features related to a-C or t-PA contamination can be seen confirming the high quality of diamond crystallites in spite of their growth in Si-rich plasma.

The mapping of intensities of the diamond Raman peak (1332 cm^{-1}) and the β-SiC peak (796 cm^{-1}) was performed on the growth surface for 50 × 50 μm^2 area in a laser beam scanning regime with the step of 1.0 μm to get information on the spatial distribution of the two components. The map shown in Fig. 5a consists of 2500 pixels and is generally similar to SEM pictures in Fig. 4e, although it was taken in a different location on the sample. The β-SiC phase occupies about 20% fraction of the whole area. To construct the Raman map of the cross-section we added the distribution of Si Raman peak (520 cm^{-1}). The resulting map (Fig. 5b) reveals the sharp film/substrate interface and demonstrates again the coexistence of diamond and SiC phases, but only on the upper part of the composite film, in agreement with SEM observation (Fig. 4c, e).

The photoluminescence spectrum for a SiC inclusion displays Raman peaks for β-SiC and strong D- and G-peaks of the Raman 1st order for amorphous sp2 carbon (Fig. 6a). Weaker and broad 2nd and 3rd order Raman peaks for sp2 carbon are present at longer wavelengths centered at ≈550 nm and 590 nm. Also, the zero-phonon line (ZPL) at 738 nm belonging to Si-vacancy (SiV) defect in diamond is seen. The SiV color center contributes to the total PL spectrum since a part of laser beam interacts with a diamond surrounding the SiC inclusion. However, the signal from SiV is relatively weak; its intensity is lower than that for the 1st order Raman spectrum for sp2 a-C. No PL specific for SiC crystals features can be seen in the spectrum in the wavelength range of 475–800 nm.

The Raman spectrum in the narrow range of 600–1100 cm^{-1} near the SiC peak at 796 cm^{-1} (see inset in Fig. 6a), brings more information about the phase purity of β-SiC component. Besides the TO-phonon

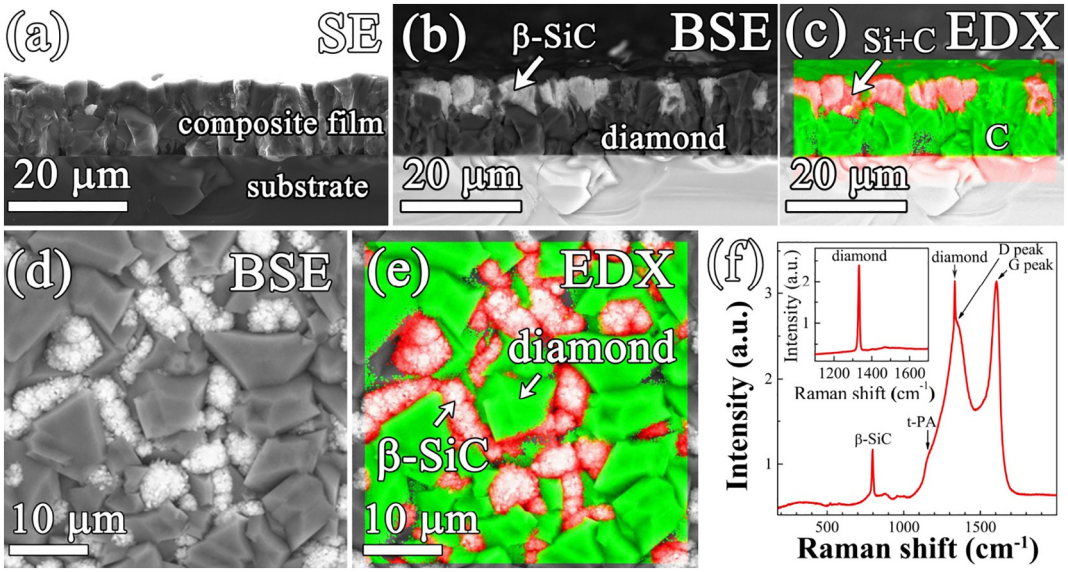

Fig. 4. SEM images of the Si/diamond/SiC-diamond structure with the 7 μm thick buffer PCD layer on the Si substrate. Cross-section structure images are taken in SE (a), BSE (b) and EDX (c) modes. SiC domains with a white (b) or red (c) contrast are revealed in the top part of the film. The plan-view of the same sample on the 40 × 40 μm^2 area as seen in SE (d) and EDX (e) modes. SiC inclusions manifest themselves by a white (d) or red (e) contrast. In EDX images (c, d) green color marks carbon, and red color denotes silicon. (f) The Raman spectrum for a SiC inclusion on the top of the Si/diamond/SiC-diamond structure. Inset: the Raman spectrum for a selected diamond grain. The excitation wavelength is 473 nm. (For interpretation of the references to color in this figure legend, the reader is referred to the web version of this article.)

mode (795.6 cm^{-1}) for the cubic SiC polytype, three weak bands belonging to 6H-SiC polytype [28] are observed: TO phonon at 766 cm^{-1} and LO phonons at 889 and 965 cm^{-1}. Therefore, a small fraction of the hexagonal polytype is present in the dominant β-SiC phase.

The PL spectrum obtained from a diamond grain of the composite is demonstrated in Fig. 6b. The SiV PL peak dominates now the spectrum, having intensity ~50 times stronger than that for the diamond Raman peak. The inset in Fig. 6b shows the zoomed PL spectrum for the diamond component to highlight the several bands, from 563 nm to 674 nm. The five bands at 563 nm (2.2 eV), 590 nm (1.91 eV), 614 nm (2.02 eV), 649 nm (2.1 eV) and 674 nm (1.84 eV) are known to be observed in some nominally undoped CVD diamond films upon green light excitation [31]. The 2.2 eV band is suggested to be ZPL for this group of bands [31]. The origin of this color center is not fully understood, its preliminary model includes a divacancy captured by an impurity atom [31], and a further study is needed to clarify this issue.

The diamond Raman peak width ($\Delta\nu$ = 8.3 cm^{-1}) for our composite is smaller than that for similar SiC-diamond composites reported by Zhuang and Jiang [19] (9.7–14.4 cm^{-1}), yet it's much larger compared to the Raman peak width (2.3–2.5 cm^{-1}) for high-quality low-stress polycrystalline diamond films and single crystals, as measured by us with the same Raman spectrometer [32,33]. The peak broadening in the spectra for the composite is thought to be caused by enhanced concentration of defects and/or nonuniform stress in the film.

3.3. Si/SiC/SiC-diamond structure

To reduce the possible stress in composite films, we tested another recipe for the SiC-diamond film growth. The first step was the formation of the textured SiC layer on (100) Si substrate before surface seeding with nanodiamond in the following regime: the total gas flow of 500 sccm, concentrations $[CH_4]/[H_2]$ = 4% and $[SiH_4]/[CH_4]$ = 20%, microwave power was 4.0 kW, pressure of 72 Torr, the substrate temperature of 775 ± 25 °C, deposition time of 1 h. No diamond seeding of the Si substrate was employed at this stage. The estimated SiC film thickness was of the order of 100 nm. This SiC interlayer served to provide the nucleation layer for the further SiC deposition along with the diamond growth. Next, the SiC surface was seeded densely with 50 nm diamond nanoparticles, and the SiC-diamond co-deposition was continued at the same regime for 20 h to produce the composite film of ≈7 μm thickness (growth rate of 350 nm/h) with β-SiC grains propagating up perpendicularly to the substrate directly from the β-SiC buffer layer.

The identification of phases in the produced composite was

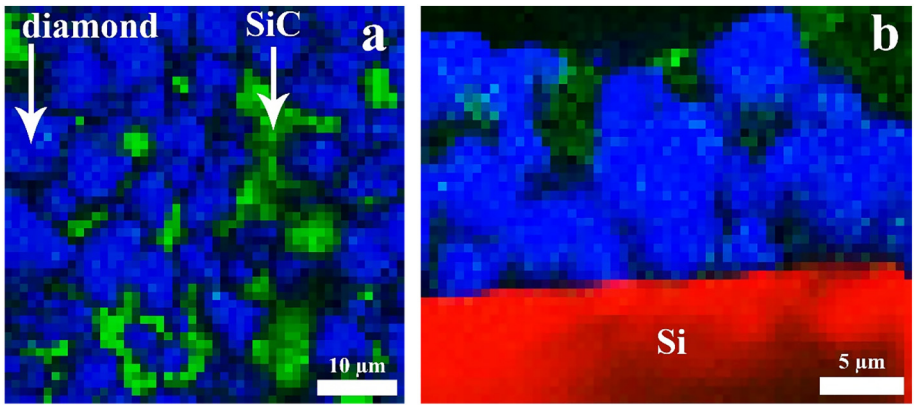

Fig. 5. Maps of Raman intensity of the diamond peak at 1332 cm^{-1} (blue color) and the SiC peak at 796 cm^{-1} (green color) on the growth surface of the Si/diamond/SiC-diamond structure (a), and in the cross-section (b). The Si substrate in (b) is shown with red color. The map area is 50 × 50 μm^2 (a) and 24 × 28 μm^2 (b). (For interpretation of the references to color in this figure legend, the reader is referred to the web version of this article.)

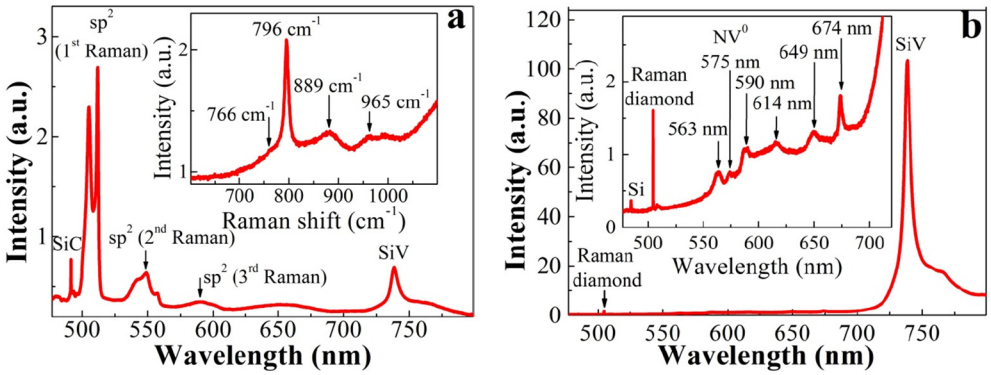

Fig. 6. (a) The photoluminescence spectrum for a SiC inclusion in the Si/diamond/SiC-diamond structure. The strong peak at 738 nm is due to Si-vacancy defect in diamond. Raman peaks for β-SiC and amorphous sp2 carbon are present at short wavelengths (< 600 nm). Inset: the Raman spectrum for a SiC inclusion in the narrow range near SiC peak at 796 cm^{-1}. (b) PL spectrum for a diamond grain. Inset: Zoomed PL spectrum shows details of a group of PL bands between 563 and 674 nm.

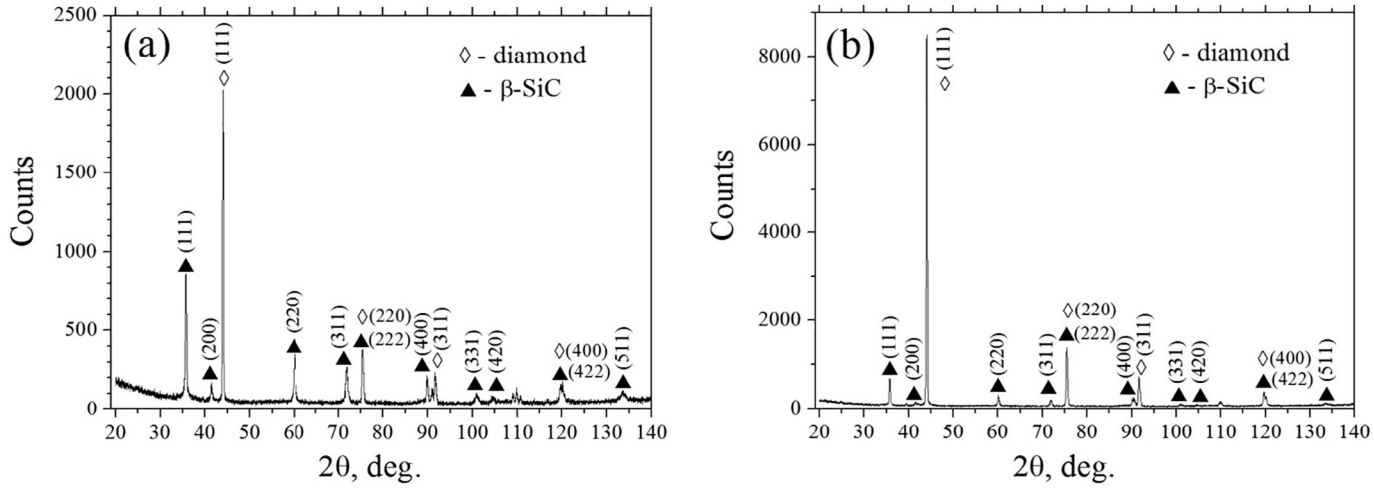

Fig. 7. XRD patterns for structures: (a) Si/SiC/SiC-diamond and (b) Si/diamond/SiC-diamond, both recorded under grazing angle α = 10°. The peaks for the diamond phase are marked with diamonds and those for β-SiC with triangles.

performed with XRD. The XRD pattern for the Si/SiC/SiC-diamond structure, taken in glancing incident diffraction (the incident angle α = 10°), is presented in Fig. 7. The X-ray penetration depth, in this case, was reduced to ~10 μm only, so the reflexes from Si, such as very strong interfering peak of (400) reflex of the (100) Si substrate between 66° and 71° observed in standard θ/2θ mode in Bragg–Brentano geometry (not shown here), have been eliminated. The XRD pattern reveals the (111), (220), (311) and (400) reflexes from diamond positioned at 44.0°, 75.3°, 91.6°, and 120°, respectively, and (111), (200), (220), (311), (222), (400), (331), (420), (422), and (511) reflexes for β-SiC positioned at 35.7°, 41.4°, 60.1°, 71.9° 75.4°, 89.8°, 100.9°, 104.6°, 120.0°, and 133.6°, respectively. The peak positions are in accordance with the XRD database for diamond (PDF-2 01-071-3649) and SiC (PDF-2 03-065-0360).

The width (FWHM) of XRD (111) peak for β-SiC is as small as 0.19° and the larger FWHM of 0.37° is measured for (200) peak (all the peak widths were measured for the XRD pattern in the θ/2θ mode). Note, that the latter value is smaller than the FWHM of the (200) reflex for hetero-epitaxial β-SiC films grown on (100) Si substrates by MPCVD using a gas mixture of TMS and hydrogen, as reported by Zhuang et al. [27], indicating a rather good crystallinity of β-SiC phase in our composite. The mean grain size (region of coherent X-ray scattering) *D* for β-SiC was estimated from the XRD peak broadening using the Debye–Scherrer formula (by selecting CuKα$_1$ component), neglecting the possible effect of the strain in the film. We found the grain size of 49 nm and 26 nm from the broadening of β-SiC (111) and (200) peaks, respectively, while for the diamond component the grain size defined in a similar way was about 150 nm. The ratio of integral intensities (area under peaks) for SiC $I_{(200)}/I_{(111)}$ is 0.63, that is 3 times larger than that for standard β-SiC powder data ($I_{(200)}/I_{(111)}$ = 0.2) [18], indicating a dominant (100) texture of the β-SiC component. The relative intensities of (111), (220) and (311) reflexes in the XRD pattern for the diamond phase are found to be close to those known for tabulated powder spectrum, thus the diamond grains are almost randomly oriented.

For comparison the XRD pattern for the Si/diamond/SiC-diamond structure described in Section is displayed in Fig. 7b. The peak ratio $I_{(220)}/I_{(111)}$ of 16:100 for diamond component indicates its (111) texture. Similarly, the dominating (111) peak and very weak (200) peak for β-SiC confirms (111) texture for the silicon carbide grains as well. The relative amount of diamond phase against to SiC phase for the sample with the diamond buffer layer is much larger compared to that for the Si/SiC/SiC-diamond sample, as seen from the reflexes intensities in the XRD pattern in Fig. 7a and b, respectively. This is explained primarily by contribution of the diamond interlayer under SiC-diamond composite to the XRD signal. By further reducing the X-ray grazing angle down to 5°, we observed an increase of SiC-diamond ratio in XRD pattern (not shown here) due to increased contribution of top composite layer to the X-ray diffraction signal. The grain sizes of 66 nm and ~150 nm for β-SiC and diamond components, respectively, were estimated from the XRD peaks broadening. Thus, for the composite with the silicon carbon interlayer the β-SiC grain size increased by a factor of 1.35 in comparison with that for the Si/diamond/SiC-diamond structure.

The characterization of Si/SiC/SiC-diamond structure with SEM and Raman spectroscopy (not given here) revealed a similarity for SiC and diamond components distribution within the film with the pictures shown earlier for the Si/diamond/SiC-diamond sample (Figs. 4d, e and 5a). Moreover, a significant improvement in crystallinity of both phases

was found. Particularly, the 1332 cm^{-1} diamond Raman peak width reduced to 3.4 cm^{-1}, and the β-SiC 795.9 cm^{-1} peak width reduced to 7.9 cm^{-1}, the latter value being very close to the width of the β-SiC epitaxial film on (111) Si grown by means of chemical interaction between mono-crystalline Si and CO gas [28]. Thus, the tuning of the parameters of the nucleation process (formation of the buffer layer of pure diamond or pure SiC), even with an invariable recipe for the further SiC-diamond co-deposition, might have a positive impact on the quality of composite components.

4. Conclusions

We demonstrated a simultaneous deposition of microcrystalline diamond and SiC in a microwave plasma using H_2-CH_4-SiH_4 mixtures at the high microwave power density and produced SiC-diamond composite films and complex layered structures on (100) Si substrates. The film structure was characterized with XRD and Raman spectroscopy, confirming the dominant silicon carbide phase in the prepared composite to be the cubic polytype β-SiC (3C-SiC) with the presence of a small fraction of the hexagonal polytype. The crystalline quality of the composite is high, as evidenced by narrow Raman peaks both for diamond (1332 cm^{-1}, FWHM = 3.4 cm^{-1}) and β-SiC (TO-phonon 796 cm^{-1}, FWHM = 7.9 cm^{-1}). The diamond grains are Si-doped due to the presence of SiH_4 in the plasma as evidenced by the strong photoluminescence of SiV color centers. Using CH_4 and SiH_4 as two separate precursors allows a very broad variation of the Si/C ratio in the gas allowing the easy tuning of diamond-SiC composite growth conditions, including the formation a proper buffer layer, such as pure SiC or pure diamond interlayer, and the achievement of similar deposition rates for the both phases.

Acknowledgments

The authors are thankful to V. Yurov for the data on absorbed microwave power density in plasma, and E. Zavedeev for optical profilometry measurements. This work was supported by RFBR, grant № 18-29-11023.

References

[1] V.V. Srikanth, X. Jiang, A. Köpf, Deposition of diamond/β-SiC nanocomposite films onto a cutting tool material, Surf. Coat. Technol. 204 (2010) 2362–2367.
[2] A.A. Shul'zhenko, E.E. Ashkinazi, A.N. Sokolov, V.G. Gargin, V.G. Ral'chenko, V.I. Konov, L.I. Aleksandrova, R.K. Bogdanov, A.P. Zakora, I.I. Vlasov, Novel hybrid ultrahard material, J. Superhard Mater. 32 (2010) 293–300.
[3] S. Yu, Z. Chen, Y. Wang, R. Luo, T. Xu, Y. Pan, J. Liao, Fabrication of SiC/diamond composite coatings by electrophoretic deposition and chemical vapor deposition, Int. J. Appl. Ceram. Technol. 14 (2017) 644–651.
[4] T. Wang, H. Zhuang, X. Jiang, One step deposition of highly adhesive diamond films on cemented carbide substrates via diamond/β-SiC composite interlayers, Appl. Surf. Sci. 359 (2015) 790–796.
[5] S.K. Gordeev, S.G. Zhukov, L.V. Danchukova, T.C. Ekstrom, Low-pressure fabrication of diamond–SiC–Si composites, Inorg. Mater. 37 (2001) 579–583.
[6] W. Zheng, X. He, M. Wu, S. Ren, S. Cao, D. Guan, R. Liu, X. Qu, Preparation and thermal conductivities of diamond/SiC composites, Appl. Phys. A Mater. Sci. Process. 124 (2018) 804.
[7] H. Zhuang, L. Zhang, T. Staedler, X. Jiang, Nanoscale integration of SiC/SiO2 core-shell nanocables in diamond through a simultaneous hybrid structure fabrication, Appl. Phys. Lett. 100 (2012) 193102.
[8] T. Wang, S. Handschuh-Wang, Y. Yang, H. Zhuang, C. Schlemper, D. Wesner, H. Schönherr, W. Zhang, X. Jiang, Controlled surface chemistry of diamond/β-SiC composite films for preferential protein adsorption, Langmuir 30 (2014) 1089–1099.
[9] I. Aharonovich, E. Neu, Diamond nanophotonics, Adv. Opt. Mater. 2 (2014) 911–928.
[10] A. Lohrmann, T.J. Karle, V.K. Sewani, A. Laucht, M. Bosi, M. Negri, S. Castelletto, S. Prawer, J.C. McCallum, B.C. Johnson, Integration of single-photon emitters into 3C-SiC microdisk resonators, ACS Photonics 4 (2017) 462–468.
[11] J. Qian, G. Voronin, T.W. Zerda, D. He, Yjj. Zhao, High-pressure, high-temperature sintering of diamond–SiC composites by ball-milled diamond–Si mixtures, J. Mater. Res. 17 (2002) 2153–2160.
[12] E.A. Ekimov, N.V. Suetin, A.F. Popovich, V.G. Ralchenko, Thermal conductivity of diamond composites sintered under high pressures, Diam. Relat. Mater. 17 (2008) 838–843.
[13] B. Matthey, S. Höhn, A.-K. Wolfrum, U. Mühle, M. Motylenko, D. Rafaja, A. Michaelis, M. Herrmann, Microstructural investigation of diamond-SiC composites produced by pressureless silicon infiltration, J. Eur. Ceram. Soc. 37 (2017) 1917–1928.
[14] Z. Yang, X. He, L. Wang, R. Liu, H. Hu, L. Wang, X. Qu, Microstructure and thermal expansion behavior of diamond/SiC/(Si) composites fabricated by reactive vapor infiltration, J. Eur. Ceram. Soc. 34 (2014) 1139–1147.
[15] C. Zhu, J. Lang, N. Ma, Preparation of Si–diamond–SiC composites by in-situ reactive sintering and their thermal properties, Ceram. Int. 38 (2012) 6131–6136.
[16] X. Jiang, C.-P. Klages, Synthesis of diamond/β-SiC composite films by microwave plasma assisted chemical vapor deposition, Appl. Phys. Lett. 61 (1992) 1629–1631.
[17] X. Jiang, V.V. Srikanth, Y.L. Zhao, R.Q. Zhang, Facet dependent reactivity and selective deposition of nanometer sized β-Si C on diamond surfaces, Appl. Phys. Lett. 92 (2008) 243107.
[18] H. Zhuang, L. Zhang, T. Staedler, X. Jiang, Highly selective diamond and β-SiC crystal formation at increased atomic hydrogen concentration: a route for synthesis of high-quality and patterned hybrid diamond/β-SiC composite film, Scr. Mater. 65 (2011) 548–551.
[19] H. Zhuang, X. Jiang, Growth controlling of diamond and β-SiC microcrystals in the diamond/β-SiC composite films, Surf. Coat. Technol. 249 (2014) 84–89.
[20] X. Jiang, H. Zhuang, H. Fu, Diamond/β-SiC composite films, Novel Carbon Materials and Composites, John Wiley & Sons, Ltd, 2019, pp. 169–203, , https://doi.org/10.1002/9781119313649.ch6.
[21] H.S. Kim, Y.J. Park, I.H. Choi, β-SiC thin film growth using microwave plasma activated CH4-SiH4 sources, Thin Solid Films 341 (1999) 42–46.
[22] V. Sedov, V. Ralchenko, A.A. Khomich, I. Vlasov, A. Vul, S. Savin, A. Goryachev, V. Konov, Si-doped nano-and microcrystalline diamond films with controlled bright photoluminescence of silicon-vacancy color centers, Diam. Relat. Mater. 56 (2015) 23–28.
[23] V.G. Ralchenko, V.S. Sedov, A.K. Martyanov, A.P. Bolshakov, K.N. Boldyrev, V.S. Krivobok, S.N. Nikolaev, S.V. Bolshedvorskii, O.R. Rubinas, A.V. Akimov, Monoisotopic ensembles of silicon-vacancy color centers with narrow-line luminescence in homoepitaxial diamond layers grown in H2–CH4–[x] SiH4 gas mixtures (x = 28, 29, 30), ACS Photonics 6 (2018) 66–72.
[24] A.P. Bolshakov, V.G. Ralchenko, V.Y. Yurov, A.F. Popovich, I.A. Antonova, A.A. Khomich, E.E. Ashkinazi, S.G. Ryzhkov, A.V. Vlasov, A.V. Khomich, High-rate growth of single crystal diamond in microwave plasma in CH4/H2 and CH4/H2/Ar gas mixtures in presence of intensive soot formation, Diam. Relat. Mater. 62 (2016) 49–57, https://doi.org/10.1016/j.diamond.2015.12.001.
[25] E.V. Bushuev, V.Y. Yurov, A.P. Bolshakov, V.G. Ralchenko, A.A. Khomich, I.A. Antonova, E.E. Ashkinazi, V.A. Shershulin, V.P. Pashinin, V.I. Konov, Express in situ measurement of epitaxial CVD diamond film growth kinetics, Diam. Relat. Mater. 72 (2017) 61–70.
[26] A.A. Smolin, V.G. Ralchenko, S.M. Pimenov, T.V. Kononenko, E.N. Loubnin, Optical monitoring of nucleation and growth of diamond films, Appl. Phys. Lett. 62 (1993) 3449–3451, https://doi.org/10.1063/1.109045.
[27] H. Zhuang, L. Zhang, T. Staedler, X. Jiang, Low temperature hetero-epitaxial growth of 3C-SiC films on Si utilizing microwave plasma CVD, Chem. Vap. Depos. 19 (2013) 29–37.
[28] J. Wasyluk, T.S. Perova, S.A. Kukushkin, A.V. Osipov, N.A. Feoktistov, S.A. Grudinkin, Raman investigation of different polytypes in SiC thin films grown by solid-gas phase epitaxy on Si (111) and 6H-SiC substrates, Materials Science Forum, Trans Tech Publ, 2010, pp. 359–362.
[29] I.I. Vlasov, E. Goovaerts, V.G. Ralchenko, V.I. Konov, A.V. Khomich, M.V. Kanzyuba, Vibrational properties of nitrogen-doped ultrananocrystalline diamond films grown by microwave plasma CVD, Diam. Relat. Mater. 16 (2007) 2074–2077, https://doi.org/10.1016/j.diamond.2007.07.007.
[30] S..-i. Nakashima, H. Harima, Raman investigation of SiC polytypes, Phys. Status Solidi A 162 (1997) 39–64.
[31] A.M. Zaitsev, Optical Properties of Diamond: A Data Handbook, Springer Science & Business Media, 2013.
[32] G. Shu, B. Dai, V.G. Ralchenko, A.A. Khomich, E.E. Ashkinazi, A.P. Bolshakov, S.N. Bokova-Sirosh, K. Liu, J. Zhao, J. Han, Epitaxial growth of mosaic diamond: mapping of stress and defects in crystal junction with a confocal Raman spectroscopy, J. Cryst. Growth 463 (2017) 19–26.
[33] A.F. Popovich, V.G. Ralchenko, V.K. Balla, A.K. Mallik, A.A. Khomich, A.P. Bolshakov, D.N. Sovyk, E.E. Ashkinazi, V.Y. Yurov, Growth of 4″ diameter polycrystalline diamond wafers with high thermal conductivity by 915 MHz microwave plasma chemical vapor deposition, Plasma Sci. Technol. 19 (2017) 035503.